PCCP

ROYAL SOCIETY OF CHEMISTRY

PAPER

View Article Online
View Journal | View Issue

Cite this: *Phys. Chem. Chem. Phys.*, 2025, **27**, 6288

High-speed imaging of non-photochemical laser-induced nucleation in aqueous cesium chloride†

Eleanor R. Barber and Andrew J. Alexander *

A study of non-photochemical laser-induced nucleation (NPLIN) of cesium chloride in aqueous supersaturated solutions is presented. Single, unfocused laser pulses (duration 5 ns, peak power density 180 MW cm^{-2}) of 532 nm laser light were used to induce crystal nucleation, and the resulting dynamics were studied using imaging at frame rates up to 250 000 frames per second (4 μs per frame). Thermocavitation events were observed in a surrounding index-matching fluid, both in the bulk and at the exterior walls of vials. These events were attributed to heating of solid particles by the laser light. The cavities were observed to oscillate in size, with the initial expansion and collapse lasting approximately 50 μs. In some cases, a small persistent gas bubble (lifetime >1 s) was observed after the cavitation event. Within the supersaturated salt solutions, new objects were observed in the image frame of the laser pulse, which faded within 20 μs. These objects were attributed to cavitation: this is the first time that thermocavitation has been observed during NPLIN using an unfocused laser pulse. Crystals were observed to grow at the locations of cavitation events, and the growth was faster at higher supersaturations. Crystals were sometimes observed to form in the location of particles that were observed before the laser pulse, which we consider to be impurity particles that trigger NPLIN. The results provide direct evidence for the nanoparticle-heating mechanism for NPLIN, which begins with thermocavitation. The possible role of stable gas bubbles in NPLIN of crystals is discussed.

Received 29th October 2024,
Accepted 3rd March 2025

DOI: 10.1039/d4cp04147j

rsc.li/pccp

1. Introduction

There are a number of techniques available for *in situ* monitoring of crystal formation and growth.[1] These include neutron and X-ray scattering methods; vibrational, infrared or Raman spectroscopy; mass spectrometry; transmission electron microscopy; and NMR spectroscopy. However, the majority of these techniques are not capable of recording data at the short timescales of initial crystal formation, which can be in the range of microseconds to milliseconds, or possibly even shorter timescales for fast crystallisation processes.[2] For time-resolved measurements, temporal control over nucleation is also required. The study of rapid crystallisation is therefore limited by the available experimental techniques, both in terms of crystallisation method and analysis technique.

Most of the fastest data in the literature for the measurement of solution structures following initiation of crystallisation comes from studies of precipitation reactions using time-resolved small- or wide-angle X-ray scattering (SAXS or WAXS, respectively).[2–9] In precipitation reactions, a sparingly soluble product forms at a high supersaturation from the addition of two reactants and rapidly crystallises. This method of crystallisation is suited to time-resolved experiments due to the moderately well-defined starting time. However, there is a mixing time as well as additional dead time determined by the apparatus before the first measurements can be made. Experimental setups are therefore carefully designed to achieve the fastest measurement time possible. Through the use of continuous flow techniques and microfluidics, measurements have been made on the timescale of microseconds. For example, Marmiroli *et al.* have studied the formation of calcium carbonate using SAXS with their first measurement taken 75 μs following the start of mixing.[8] The fastest initial measurement reported currently was recorded by Schmidt *et al.* for the formation of zinc sulfide.[9] A liquid jet of aqueous zinc chloride was injected into an atmosphere of flowing hydrogen sulfide gas, which quickly diffused into the solution. The first SAXS measurement was taken after 17 μs.

Laser-induced nucleation (LIN) techniques have the potential to allow access to measurements at even shorter timescales than precipitation reactions, due to the lack of mixing time or dead time. Although LIN has been used in multiple studies for the real-time analysis of crystal formation and growth,[10–20] fast measurements have been carried out in only a few instances. Growth dynamics of potassium nitrate from supersaturated aqueous solutions were studied by Jacob *et al.*[21] following initiation of

School of Chemistry, University of Edinburgh, David Brewster Road, Edinburgh, Scotland, EH9 3FJ, UK. E-mail: andrew.alexander@ed.ac.uk

† Electronic supplementary information (ESI) available. See DOI: https://doi.org/10.1039/d4cp04147j

nucleation by a focused laser pulse. The process was monitored by the measurement of light transmitted through the sample by a xenon lamp; turbidity due to the scattering from the crystal nuclei was measured as a function of time. Using this technique, measurements were made at times shorter than 1 ms. However, measurements were limited to the millisecond timescale due to the low molar turbidity coefficient of the system. Optical imaging can achieve faster measurements. For example, high-speed optical imaging has been used to observe laser-induced cavitation (using a focused laser pulse) and subsequent crystal nucleation on a microsecond timescale.[22–28]

Non-photochemical laser-induced nucleation (NPLIN) typically uses unfocussed pulses of laser light, with durations on the order of nanoseconds, to initiate crystal nucleation.[29,30] The use of low pulse energies, with visible or near-infrared wavelengths, prevents photochemical damage to the target material. There have been a number of studies aimed at determining the possible mechanisms for NPLIN.[30–32] The current understanding favours the nanoparticle heating (NPH) mechanism. In this mechanism, the laser light is absorbed by trace solid nanoparticles, which results in rapid heating to a high temperature, spontaneous vaporization of the surrounding fluid, and subsequent collapse of the cavity, *i.e.*, thermocavitation. It is not clear, however, what stage of the thermocavitiation event causes crystal nucleation. For example, the expansion of a cavity involves a hot gas–liquid interface, where solvent evaporation could cause local increases in supersaturation.[28,33–35] Alternatively, collapse of a cavity is expected to produce pressure waves, with regions of higher density and therefore higher supersaturation. A cavitation bubble is transient because the hot vapor cools rapidly, typically within tens of microseconds, and the resulting internal pressure is insufficient to maintain the void. A gas bubble, by comparison, has sufficient internal pressure to be stable and persist for some time. In a recent study, Barber *et al.* demonstrated that thermocavitation during NPLIN can lead to production of gas bubbles, and that these may be involved in the nucleation of crystals.[36]

In the present work, we report on results from high-speed imaging of cesium chloride crystals following NPLIN with a single, unfocussed laser pulse. The primary objective was to optimise the frame rate and imaging conditions in order to view crystals as soon as possible after the laser pulse. Imaging was carried out at frame rates up to 250 000 frames per second (4 μs per frame). In some cases, nucleation was observed to occur at particles that were present prior to the NPLIN pulse, supporting the NPH mechanism. The results reveal the formation of a cavity that precedes the rapid growth of a crystal.

2. Experimental methods

Cesium chloride was used because of its high solubility in water at room temperature, and the high refractive index (1.640 at 590 nm) of the solid, which aids in contrast for imaging. Supersaturated aqueous solutions of cesium chloride were prepared by dissolution of the solid (Sigma Aldrich, ≥98%) in ultrapure water (18 MΩ cm). Samples with concentrations (C) of 11.9 and 13.1 mol kg^{-1} (molality) were made by dissolution at 65–70 °C, and then transferred into glass vials (diameter 11.6 mm, approximately 1.5 cm^3) without filtration. Samples were cooled to temperatures of 21 or 25 °C, at which the saturation concentrations (C_{sat}) of cesium chloride are 11.1 and 11.4 mol kg^{-1}, respectively.[37] Details of the cooling method are given in the ESI.† The resulting supersaturations ($S = C/C_{sat}$) ranged from 1.05 to 1.18.

Samples were exposed to a single pulse of laser light (pulse duration 5.0 ns) from a Q-switched Nd^{3+}:YAG laser (Continuum Surelite II-10). Visible laser light (532 nm) was used to simplify alignment of beams within the imaging setup. The beam diameter was 3 mm and the incident pulse energies were 65–70 mJ; corresponding to pulse energy densities of 920–990 mJ cm^{-2} and peak power densities of 173–186 MW cm^{-2}. After samples had been nucleated, they were regenerated by heating to be used again.

The peak laser power densities used in the present work (173–186 MW cm^{-2}) are commensurate with previous studies of NPLIN for aqueous solutions of KCl (0.5–100 MW cm^{-2}), NaBr (100–450 MW cm^{-2}), urea (20–350 MW cm^{-2}), glycine (80–910 MW cm^{-2}), and sodium acetate (5–68 MW cm^{-2}).[31,36,38] These power densities are three orders of magnitude lower than the experiments of Yoshikawa *et al.* (∼PW cm^{-2}), who used focussed fs pulses to induce breakdown of the fluid, resulting in cavitation and bubble formation.[33,34]

Details of the imaging setup are given in the ESI.† Imaging of crystal growth following NPLIN was carried out first using a low-speed digital camera (Basler, acA2040-90um) and then using a high-speed camera (Photron FastCam SA1.1), each equipped with a zoom-lens. The maximum framerates used were 700 and 250 000 fps for the low and high-speed cameras, respectively. The sample was immersed in a bath of refractive index-matching fluid (mineral oil, refractive index 1.42–1.43) to improve the image quality.[37] Sample vials were imaged from two directions: from the side, with the camera aligned perpendicularly to the NPLIN laser beam, and from the front, with the camera at a shallow angle to the beam (Fig. S1, ESI†). A notch filter (Semrock NF01-532U-25) was used to block the 532 nm pulsed laser light. With the low-speed camera, the system was illuminated using a continuous-wave (CW) diode laser (488 nm, Cobalt 06-MLD or Lasertack LDM-488-55-C). The maximum power of the CW laser beam was 80 mW and the beam diameter was approximately 1 mm. With the high-speed camera, sample vials were imaged only from the side direction, illuminated using a white light-emitting diode (LED) positioned at a downward angle with respect to the sample vial (Fig. S2, ESI†). At higher frame rates (>54 000 fps) the LED was shone through the sample directly into the camera, and therefore crystals in the resulting images appeared as dark objects against a light background.

3. Results

3.1 Millisecond timescale

Imaging from side position. In images recorded with the low-speed camera in the side position, the frame containing the

NPLIN laser pulse could sometimes be identified from leakage of 532-nm light through the notch filter. However, it was also observed that new objects external to the vial, *e.g.*, stuck to the outside walls, appeared as a result of the NPLIN laser pulse (Fig. 1) and remained illuminated by the CW laser. After 0.2 s, these objects had decreased in intensity, but remained visible for up to 1.2 s. Based on previous work, we identify these objects as gas bubbles nucleated by the laser pulse.[36] Fig. 1 also shows a single crystal that was nucleated in the bulk solution, observed in the same frame as the laser pulse. At 250 fps, the exposure time per frame was 3864 μs, therefore this particle must have formed within 3.9 ms of the initiating pulse. Generally, only one or two crystals were observed in the first frame, with further crystals becoming visible in later images. At 700 fps, crystals were first observed growing on the vial walls at 1.3 ms after the laser pulse (Table S2, ESI†).

The brightness of crystals in some cases appeared to fluctuate from frame to frame (*e.g.*, Fig. S4, ESI†). This was at first considered to be due to rotation of anisotropic crystals. However, inspection of images taken before the NPLIN laser pulse showed that stationary dust particles on the outer vial walls also fluctuated in brightness. The fluctuations were therefore attributed to the imaging setup, *e.g.*, due to the illuminating light source.

Imaging from front position. In Fig. 2(a), bright spots (1 mm) were observed where the CW illumination beam entered (right) and exited (left) the vial, with the space between being the beam pathway through the solution. The perspective when viewing samples from the front position is illustrated schematically in Fig. S3 of the ESI.† The NPLIN laser beam propagated in the opposite direction to the CW beam, and the entry and exit points became brighter during the image frame of the pulse. The focal plane of the camera was adjusted to be in the solution behind the vial wall at the entry point of the NPLIN pulse. A group of 3 crystals was observed growing from the location of particles that were already visible before the NPLIN pulse: see Fig. 2(b). As the crystals grew, their size and brightness gradually increased, and eventually the star-like (dendritic) shapes of the crystals became apparent. The fractal habit of the crystals results from the initially high supersaturation causing rapid anisotropic growth.[39] It can also be seen that there was one object prior to the laser pulse that did not result in a crystal.

Images taken from the front position were also recorded at an increased magnification. This was not possible with the

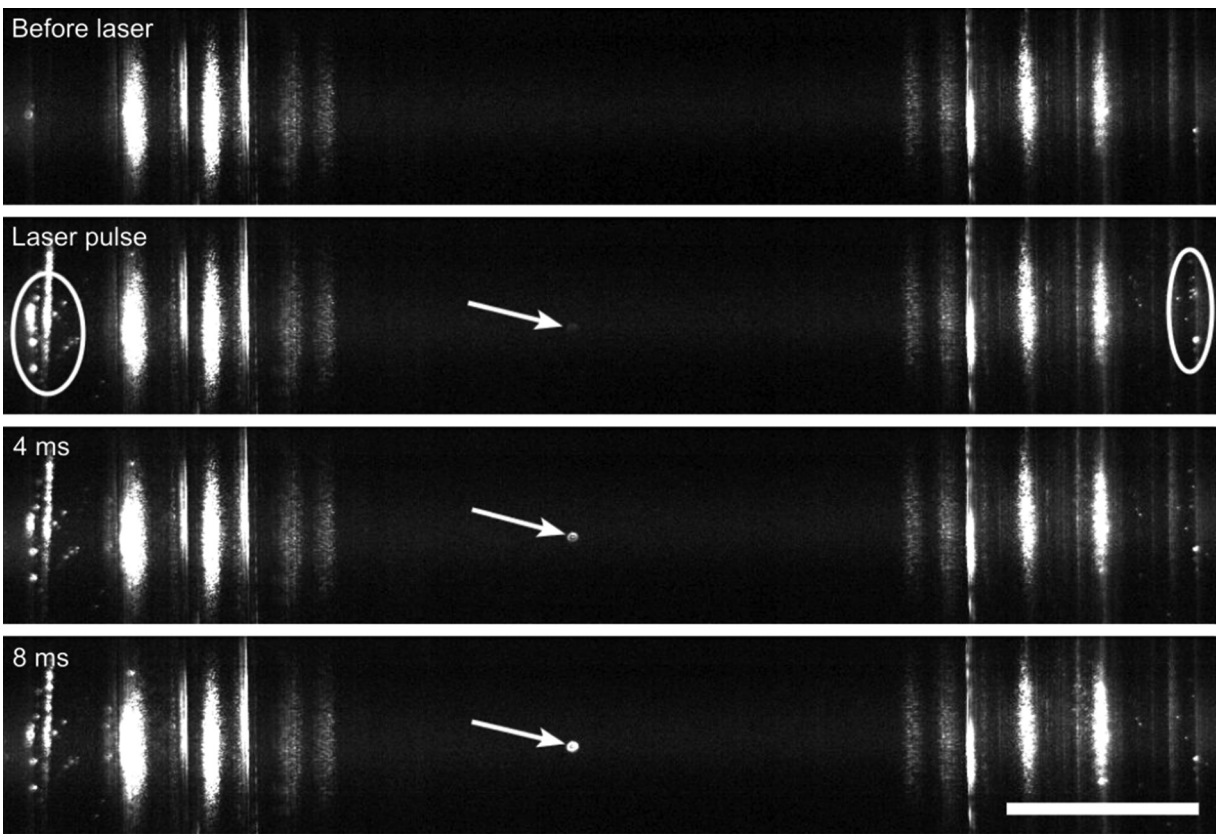

Fig. 1 Growth of a cesium chloride crystal (indicated by white arrow) in a supersaturated aqueous solution (C = 11.9 mol kg^{-1}, S = 1.05) following NPLIN. Four consecutive image frames are shown (250 fps, exposure time 3.9 ms). The top image (before the laser pulse) shows multiple reflections of the 488 nm CW illuminating laser light due to the curved walls of the vial. The incident NPLIN laser pulse (5.0 ns, 532 nm) had an energy density of 950 mJ cm^{-2}. The laser pulse occurred in the second image, evident by the illumination of dust on the outer vial walls (circled), and a particle is already visible in the centre of the vial. Subsequent images show further growth of the crystal. Brightness and contrast levels in images have been adjusted for clarity. Scale bar represents 2 mm.

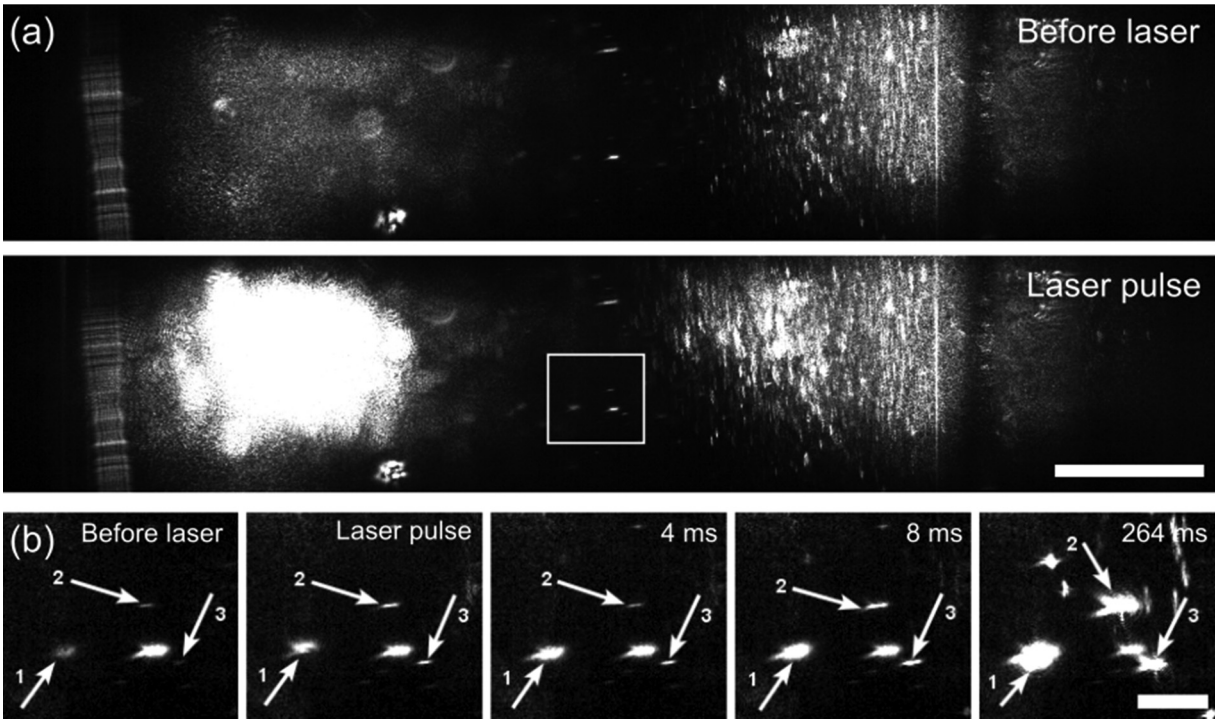

Fig. 2 Growth of cesium chloride crystals from a supersaturated aqueous solution (C = 11.9 mol kg^{-1}, S = 1.05) following NPLIN. The incident laser pulse (5.0 ns, 532 nm) had an energy density of 990 mJ cm^{-2}. The frame rate was 250 fps and the exposure time was 3.9 ms. (a) In the top image, the bright area on the left side is the exit point of the CW laser from the vial, while the area on the right is the entry point. The area on the left lights up in the bottom image as it corresponds to the entry point of the pulsed laser. (b) Four consecutively recorded images (from left to right) followed by an image recorded 264 ms after the laser pulse, showing a close-up view of the area inside the white box outlined in (a). The NPLIN laser pulse occurred in the second image. Three crystals grow from the location of three particles that were already present before the laser pulse, indicated by numbered arrows. Scale bars represent (a) 1 mm, (b) 200 μm.

camera in the side position because, as noted above, the external vial walls were important for determining the timing of the laser pulse. At increased magnification, the depth of field is decreased. However, with some trial and error, focussing was achieved that revealed the star-like shapes of crystals at sizes $<$100 μm, as shown in Fig. 3.

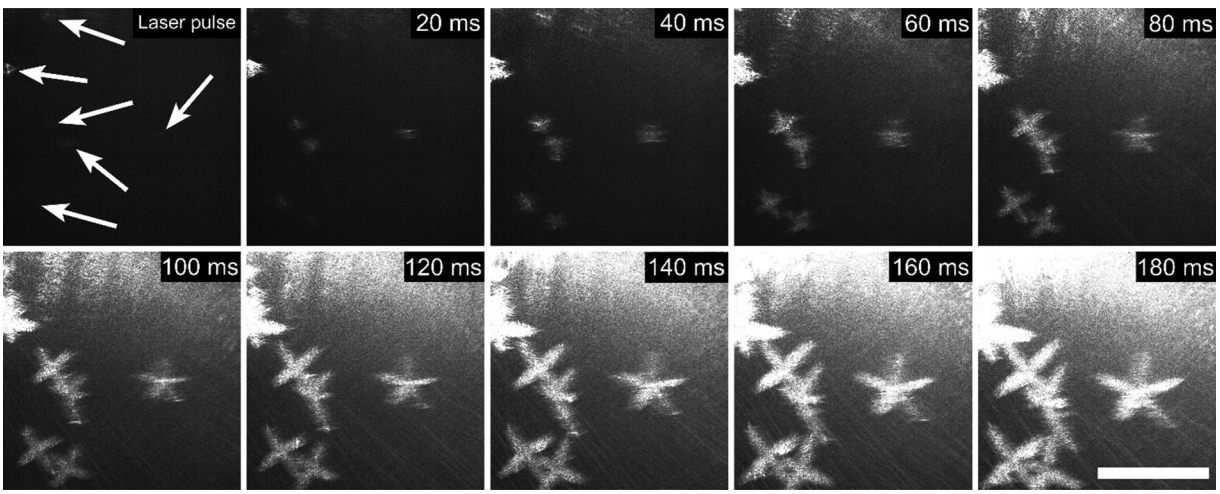

Fig. 3 Growth of cesium chloride crystals from a supersaturated aqueous solution (C = 11.9 mol kg^{-1}, S = 1.05) following NPLIN. The incident laser pulse (5.0 ns, 532 nm) had an energy density of 990 mJ cm^{-2}. Starting from the top left, the first image was taken within 8 ms of the laser pulse and the time between images is 20 ms. Of the seven crystals that formed, 6 of these were visible in the first image (white arrows). The star shape of the crystals is apparent within 40 ms. Brightness and contrast levels of the images have been optimised for clarity. Scale bar represents 500 μm.

3.2 Microsecond timescale

In images recorded in the side position with the high-speed camera, particles were observed to appear in the same frame as the laser pulse, both in the bulk solution and on the vial inner walls. The particles gradually increased in brightness and size until they were clearly identifiable as crystals, as illustrated in Fig. 4. Crystals were sometimes observed to grow from the location of particles that were present in the solution before the laser pulse. Usually only a small proportion of crystals that became visible in later images could be seen in the first frame.

At higher frame rates, images were recorded with the LED shining directly into the camera. As crystals grow, they appear darker due to blocking more light, as demonstrated in Fig. 5(a). Objects were observed in the first or second frame after the laser pulse. These objects then faded, sometimes to the extent that they were no longer visible, and they did not grow back to their initial size until tens or hundreds of milliseconds later, depending on the sample supersaturation.

At the highest frame rate used (250 000 fps) faint objects were observed in the same frame as the laser pulse: but by the next frame, the objects had faded. These objects must have formed within 4 μs of the initiating laser pulse. This behaviour was observed in both the bulk solution and on the inner vial wall. Fig. 5(b) shows an example of this in the bulk solution. After approximately 10 ms, particles were observed growing in the same locations, and they increased in size until they were clearly identifiable as crystals. These observations are consistent with the formation and collapse of thermocavities prior to crystal nucleation, supporting the NPH mechanism for NPLIN. This is the first time thermocavitation has been observed during NPLIN using an unfocused laser pulse. It should be noted also that no particles were intentionally doped into these solutions. The active nanoparticles are expected to be impurities in the as-purchased cesium chloride salt, possibly iron oxide.[14]

It was observed that crystals grew at a much faster rate in samples with a higher supersaturation. In order to quantify this, image analysis software (Fiji) was used.[40] The 8-bit binary greyscale images consist of pixels which are one of 256 possible shades of grey, from 0 (black) to 255 (white). The minimum grey value of pixels in the area of growth for a single crystal was recorded for every frame. This method gives an indication of how quickly the crystal is growing. Crystals chosen for analysis were those which grew from an object that appeared in the first frame. Fig. 6 shows a comparison between the growth of crystals in S = 1.07 (11.9 mol kg^{-1}) and 1.18 (13.1 mol kg^{-1}) solutions at 21 °C (note the changes in scale along the time axis for this graph).

Both samples show a small oscillation in the data with a period of about 11 μs, which we attribute to fluctuations in the imaging setup. During the frame in which the laser pulse occurs there is a rapid transient decrease in minimum grey value due to the formation of an object, which we assume to be a cavity. For the S = 1.07 sample, in the following frame, the grey value returns to approximately the same level as before the laser pulse, and does not decrease significantly over the next 17 ms. At about 400 ms after the laser pulse, the grey value shows a clear monotonic decline, indicating continuous growth of an object, later identified as a crystal. In the final image recorded, 1940 ms after the laser pulse, the maximum dimension of the crystals in the sample at S = 1.07 was 80 μm.

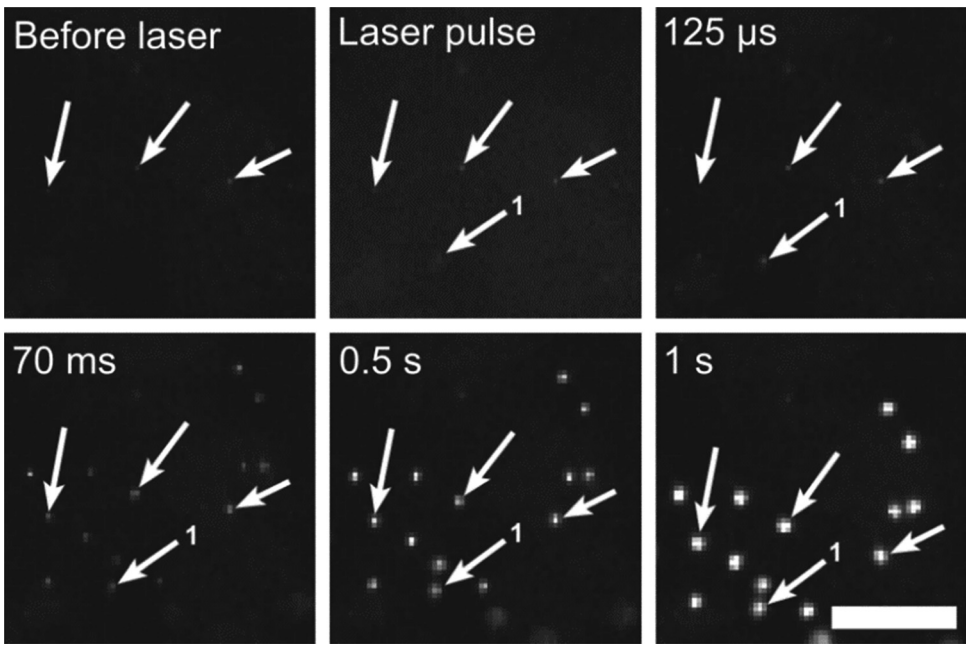

Fig. 4 Growth of cesium chloride crystals from a supersaturated aqueous solution (C = 11.9 mol kg^{-1}, S = 1.05) following NPLIN. The incident laser pulse (5.0 ns, 532 nm) had an energy density of 920 mJ cm^{-2}. The frame rate was 8000 fps (each frame 125 μs). Three crystals grow from particles which were present in the solution before the laser pulse (unlabelled arrows). The arrow labelled 1 shows an example of a single crystal nucleated where no particle was observed prior to the laser pulse. Later, other crystals become visible. Scale bar represents 400 μm.

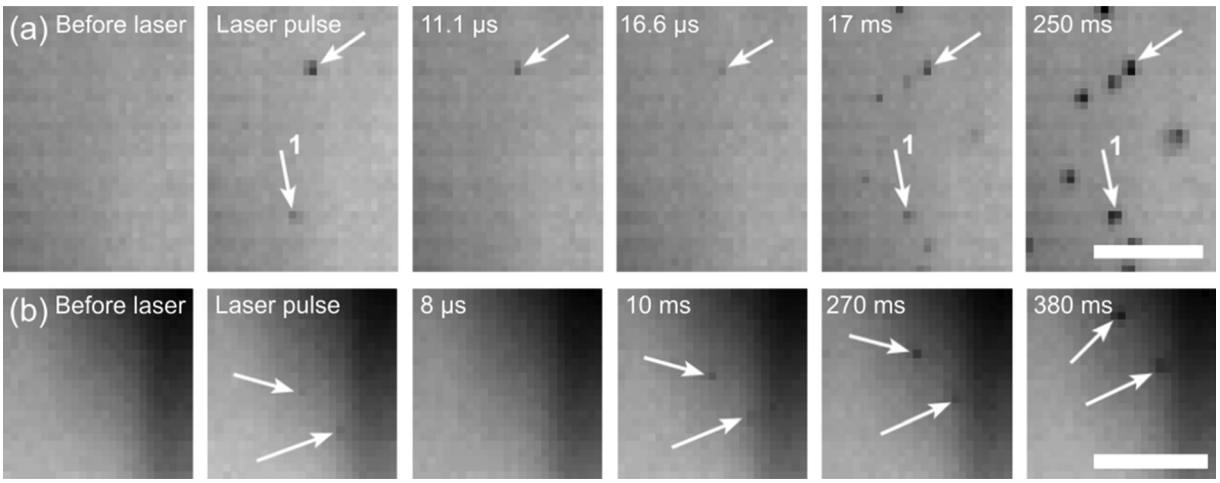

Fig. 5 Growth of cesium chloride crystals in bulk supersaturated aqueous solutions following NPLIN, recorded at different frame rates. (a) Frame rate 180 000 fps (each frame 5.6 μs), C = 13.1 mol kg^{-1}, S = 1.18. Two objects appear in the same frame as the laser pulse (indicated by arrows). The objects fade in intensity over the next 11 μs, one remaining visible (top arrow) and one disappearing from view (arrow labelled 1), and then slowly grow again until they are clearly identifiable as crystals. After 17 ms, other crystals have formed where no objects were previously observed. (b) Frame rate 250 000 fps (each frame 4 μs), C = 11.9 mol kg^{-1}, S = 1.07. Two objects appear in the same frame as the laser pulse (white arrows) but are no longer visible in the next frame. After 10 ms, two particles are visible growing in the same locations and gradually increase in size until they are clearly identifiable as crystals. In this particular case, the crystals move upwards as they grow, rather than falling down, probably due to a convection current within the sample vial. Scale bars represent 300 μm.

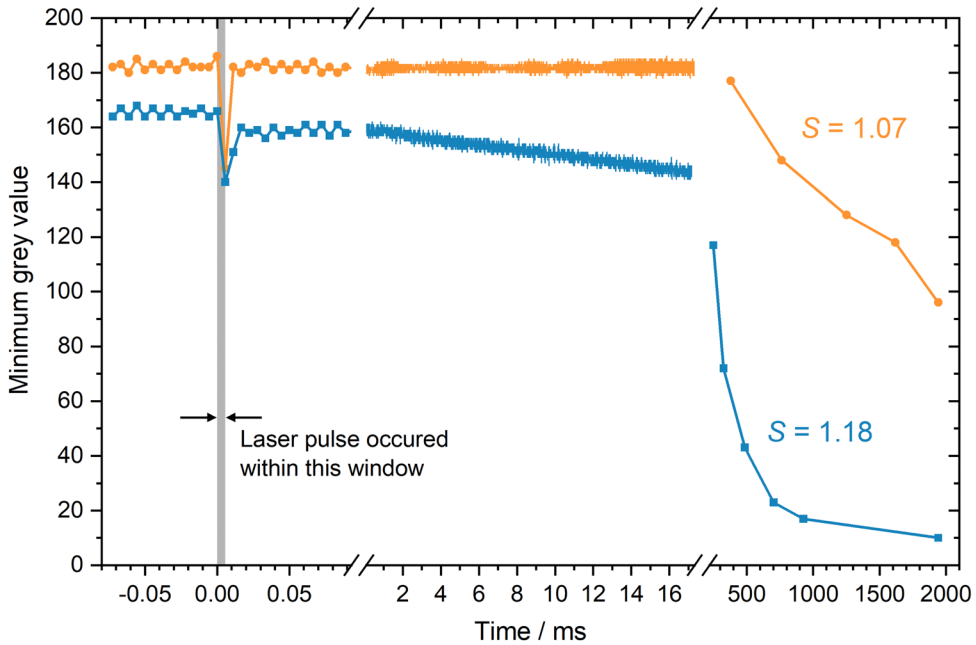

Fig. 6 Plots showing the minimum grey values of pixels from images taken from areas corresponding to a single cesium chloride crystal as a function of time after the laser pulse. The camera frame rate was 180 000 fps. Lower values represent darker pixels, resulting from less illuminating light reaching the camera. The crystals chosen each grew from an object that appeared in the first image frame. The frame in which the NPLIN laser pulse was observed is plotted at 5.6 μs. The two plots represent the crystal growth in solution with different concentrations: C = 11.9 mol kg^{-1}, S = 1.07 (orange, circles) and C = 13.1 mol kg^{-1}, S = 1.18 (blue, squares). Note the changes in timescale along the horizontal axis.

For the sample at S = 1.18, the grey value does not return to the same level as before the laser pulse, but gradually decreases over the next 17 ms, indicating that this object is continuously growing and is later identifiable as a crystal. At long times (>500 ms) the grey value begins to level off, not because the crystal has stopped growing, but because it has grown sufficiently large to block almost all of the light for the area selected for analysis. At 700 ms after the laser pulse, the crystals in the

sample at S = 1.18 were approximately 300 μm in dimension. After this time, it was not possible to measure the crystals because they overlapped each other in the images.

3.3 Cavitation on the outside of vial walls

With illumination directly into the camera, the appearance of objects on the outside vial walls (Section 3.1) was seen to be due to cavitation. Cavities were observed to form both on the outer walls of the vials and floating within the index-matching oil, either in the same frame as the laser pulse or in the next frame, as shown in Fig. 7. In Fig. 7(a), a large cavity (500 μm) was observed to grow rapidly within the first 3 frames (40 μs) following the laser pulse. The cavity collapsed, before growing back, and continued to oscillate in size. Fig. 7(b) shows a larger cavity split into two smaller cavities, before reforming into a single cavity. Larger cavities formed mainly on the surface of the outer vial wall, but were sometimes observed in the mineral oil, as shown in Fig. 7(c). It is also clear from Fig. 7(c) that cavitation can lead to small gas bubbles that persist for tens of milliseconds.

Fig. 8 shows the time dependence of the cavity diameter for the event shown in Fig. 7(a). The oscillatory behaviour during the collapse of cavitation bubbles is well known: the period of oscillation depends on the liquid density, vapour pressure, diameter of the cavity, and the proximity to a solid boundary.[41] Laser-induced cavitation is usually achieved using focused laser pulses, and has been most often studied in water.[25,42–45] The cavity collapse generally occurs on a longer timescale to that observed here, *i.e.*, hundreds compared to tens of microseconds. Due to the lower energy density of unfocused laser pulses used here, the cavities are smaller, resulting in a shorter oscillation period.

4. Discussion

The observation of cavitation bubbles outside the vial gives us confidence in identifying the first objects that form in the cesium chloride solutions as cavitation bubbles. Moreover, it was possible in some cases to link the cavitation to a particle observed in the frames before the laser pulse. Crystals were subsequently observed growing at the location of cavitation events. These are significant results, since they provide direct evidence of the particle heating mechanism for NPLIN.

The cavitation bubbles that formed in the mineral oil reached sizes of up to 500 μm in diameter, with periods of oscillation on the order of tens of microseconds. The small bubbles observed after cavitation sometimes survived for longer than one second before they disappeared, suggesting that they contained some gas. The cavities that formed in the supersaturated solutions were visible for $<$20 μs, and were too small to accurately measure, being visible only as a few pixels. There are several possible reasons for the differences in cavitation observed inside *versus* outside the vial. The impurity particles outside are likely to be larger, *e.g.*, dust particles, resulting in the vaporization of a larger amount of liquid, and larger maximum diameter of bubble.[46] The dynamics of cavity

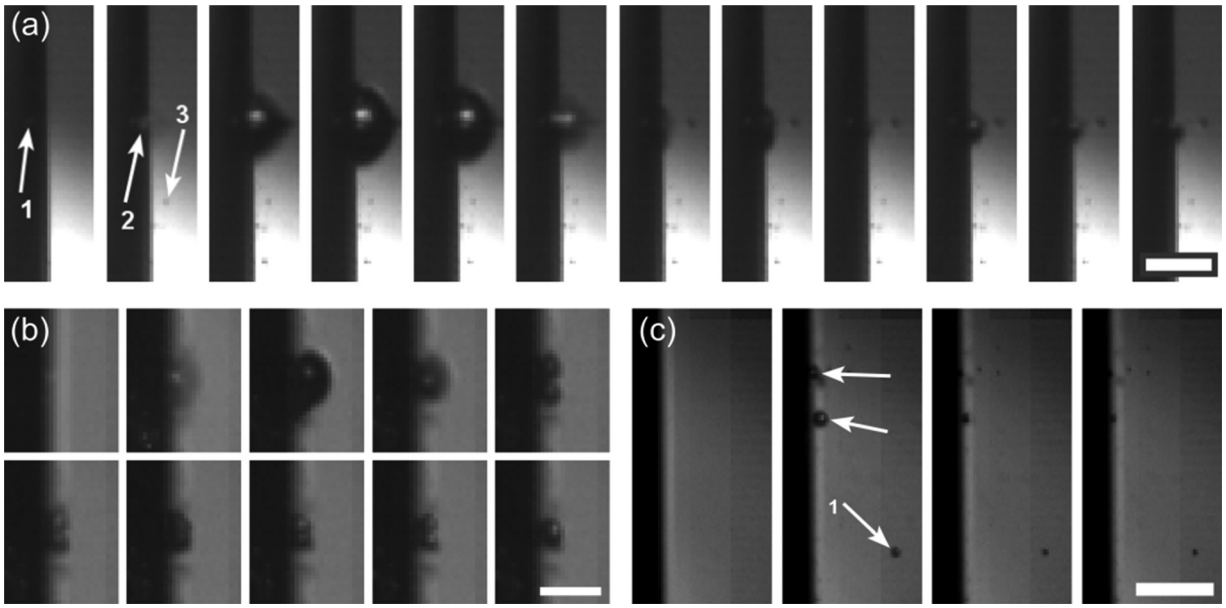

Fig. 7 Images of cavitation bubbles on the outside walls of glass vials immersed in mineral oil, following exposure to a laser pulse with an energy density of 920 mJ cm^{-2}. In each set of images (a) to (c), the laser pulse occurred in the second frame. (a) Formation of a large cavity, which oscillates in size. Consecutive images with 10 μs between frames. Before the pulse, an object was observed on the surface of the glass (arrow 1); in the same frame as the laser pulse, a cavity started to form in the same location (arrow 2). The cavity grows to a maximum diameter of 500 μm before collapsing and oscillating in size. Smaller cavities also formed in the oil (*e.g.*, arrow 3). (b) Fragmentation of a cavity into two smaller cavities before recombining. Consecutive images with 8 μs between frames; the last two images were recorded 650 and 740 μs after the laser pulse. (c) Formation of persistent gas bubbles both on the glass surface (unlabelled arrows) and within the mineral oil (arrow 1). Consecutive images with 8 μs between frames; the last image was recorded 40 ms after the laser pulse. Scale bars represent (a) 400 μm, (b) 200 μm, (c) 400 μm.

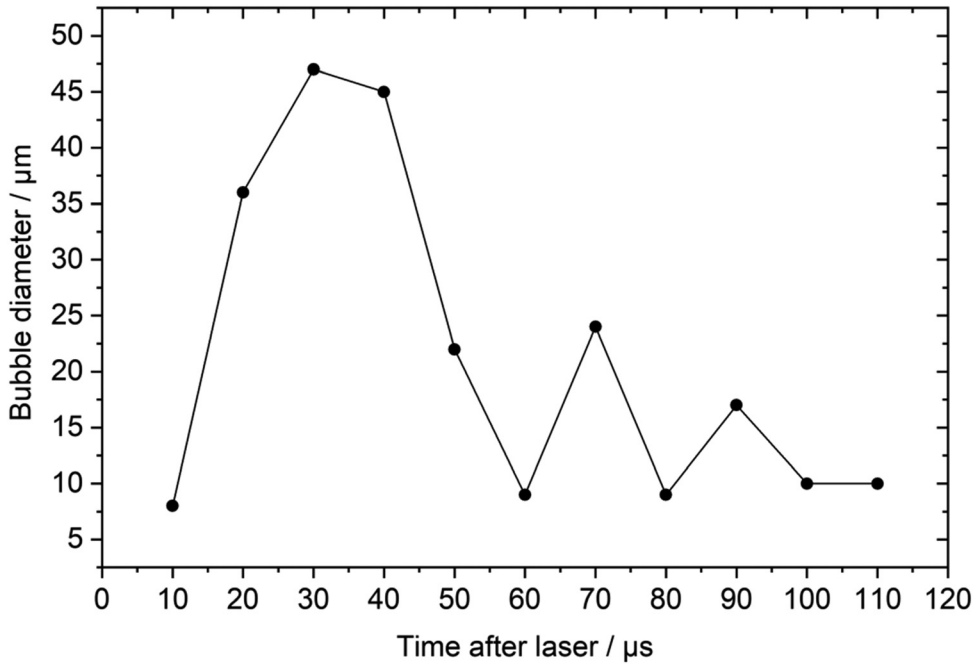

Fig. 8 Cavitation bubble diameter as a function of time, measured for the largest bubble that formed in the mineral oil on the outer vial wall, shown in Fig. 7(a). The first period of bubble growth and collapse (50 μs) is longer than the periods of the second and third oscillations (20 μs).

growth and collapse are complex, and the effects of the liquid properties are not easy to quantify.[42,47,48] One critical factor is surface tension: a larger surface tension can support a smaller bubble radius.[49] Conditions which lead to a faster collapse time are a high surface tension and low viscosity.[49,50] The cesium chloride solution has a higher surface tension and lower viscosity than the mineral oil, therefore we would expect smaller cavities that collapse faster in solution, as was observed in our experiments.

The small sizes of the growing objects observed in solution meant that it was not possible to identify them as crystalline until they reached a size large enough so that either their non-spherical shape became apparent, or they began to sediment. As noted above, the transient objects that appeared after the laser pulse were attributed to thermocavitation bubbles. It is notable, however, that persistent gas bubbles were observed in the mineral oil (Fig. 7(c)) that remained visible for up to 1.2 s following irradiation. As we have discussed previously, the origin of this gas could be either air that was already dissolved in the liquid, or gaseous reaction products resulting from the high temperatures (>1000 K) of the heated nanoparticles.[36] These observations lead us to three possible routes for NPLIN:

(1) Thermocavitation leading directly to nucleation as solute is accumulated at the expanding cavity interface.

(2) Thermocavitation; incomplete collapse of the cavitation bubble due to the formation or influx of gas; formation of a gas bubble; crystal nucleation at the bubble interface.

(3) Thermocavitation; collapse of the cavitation bubble causing immediate crystal nucleation.

Whether a persistent gas bubble in scenario (2) is involved in the crystal nucleation, or simply a bystander, is not clear. The majority of crystals observed in images such as Fig. 5(a) could not be associated with a cavitation event. We have found that if the lighting or focus is not sufficient, then objects are not visible in our setup. We also expect a range of nanoparticle sizes, with smaller particles producing cavitation events that were possibly too weak for us to observe.

We cannot rule out that there are other mechanisms for NPLIN that do not involve cavitation. Knott *et al.* have shown that the peak laser powers (180 MW cm^{-2}) used in the present experiments with nanosecond laser pulses are insufficient to cause alignment of molecules.[51] It is not clear whether there is any structuring of CsCl at the interface of impurity nanoparticles prior to the laser pulse, which may assist in the nucleation process. However, solutions can remain supersaturated for days without nucleating.

We consider whether photochemical reactions occur together with simple heating of the nanoparticles. Measurements of the nucleation probability for aqueous halide salts have shown a linear dependence with laser power, ruling out non-linear multiphoton absorptions: for example, a 2-photon photochemical process would be expected to show a quadratic dependence on laser power. Previous work on NPLIN of potassium chloride showed no significant difference in the nucleation probability (sample lability) at 532 nm and 1064 nm, suggesting that resonant electronic transitions are not involved. Moreover, NPLIN has been achieved by intentional doping of a range of nanoparticles, including Fe_3O_4, Au, Ag, 316 steel, copper phthalocyanine and CB_4.[14,52,53] This also suggests a mechanism that is independent of any electronic states of the impurity. We note that the previous observations of a threshold to the laser power at which NPLIN becomes possible, is consistent with the

requirement for a threshold temperature for thermocavitation, *i.e.*, the spontaneous vaporization of fluid.

The fastest studies of crystal nucleation and growth up to now have been mostly based on fluid mixing, creating uncertainty in the start time. The resulting high, and undefined, supersaturations rely on specific methods such as precipitation of low-solubility products, where the nucleation mechanism may be different, *e.g.*, possibly *via* non-crystalline solid intermediates. For the present work, with well-defined supersaturations, a single 5 ns laser pulse starts a sequence of events that begins with a cavitation event completed within 20 μs. The cavitation results in an object that grows continuously (faster or slower depending on supersaturation) until a crystal is clearly identified. The method we have described opens up opportunities to study the earliest events in the crystal nucleation process for a range of solute and molten systems.

5. Conclusions

High-speed imaging of NPLIN in supersaturated aqueous solutions of cesium chloride has been carried out. Using a low-speed digital camera, growing particles were observed within 3.9 ms of the laser pulse in the bulk solution, and within 1.3 ms of the laser pulse in solution at the vial walls. Using a high-speed camera, large thermocavitation bubbles (up to 0.5 mm diameter) were observed to form in the index-matching oil surrounding the vials, with the initial expansion and collapse lasting approximately 50 μs. In some cases, persistent gas bubbles with lifetimes >1 s were observed after cavitation. Within the bulk CsCl solutions, objects appeared within 4 μs of the laser pulse, which then faded within about 20 μs. These were attributed as thermocavitation events, and crystals were later observed to grow in the same locations. Additionally, both bubbles (on the outside of the vials) and crystals (in the solutions) were sometimes observed to form in the location of particles that were observed before the laser pulse, which we consider to be the impurity particles that trigger NPLIN. Altogether, these observations make for compelling evidence in favour of the particle-heating mechanism for NPLIN in aqueous cesium chloride, in which thermocavitation occurring at impurity particles is the cause of crystal nucleation. It is not clear whether the cavitation induces crystal nucleation directly, or whether there is an intermediate stage involving persistent gas bubbles.

Data availability

Data employed in this study are available *via* the Edinburgh DataShare repository (**https://datashare.ed.ac.uk/handle/10283/749** and DOI: **10.7488/ds/7887**).

Conflicts of interest

There are no conflicts to declare.

Acknowledgements

We are grateful to the Engineering and Physical Sciences Research Council (EPSRC EP/N509644/1) and to the CMAC Future Manufacturing Research Hub (**https://www.cmac.ac.uk**) for supporting this work.

References

1 N. Pienack and W. Bensch, *In Situ* Monitoring of the Formation of Crystalline Solids, *Angew. Chem., Int. Ed.*, 2011, **50**, 2014–2034.
2 R. T. Kügler, S. Doyle and M. Kind, Fundamental insights into barium sulfate precipitation by time-resolved *in situ* synchrotron radiation wide-angle X-ray scattering (WAXS), *Chem. Eng. Sci.*, 2015, **133**, 140–147.
3 M. J. Quayle, R. J. Davey, A. J. McDermott, G. J. T. Tiddy, D. T. Clarke and G. R. Jones, *In situ* monitoring of rapid crystallisation processes using synchrotron X-ray diffraction and a stopped-flow cell, *Phys. Chem. Chem. Phys.*, 2002, **4**, 416–418.
4 J. Bolze, B. Peng, N. Dingenouts, P. Panine, T. Narayanan and M. Ballauff, Formation and Growth of Amorphous Colloidal $CaCO_3$ Precursor Particles as Detected by Time-Resolved SAXS, *Langmuir*, 2002, **18**, 8364–8369.
5 H. Amenitsch and B. Marmiroli, Time-resolved structure investigation with small angle X-ray scattering using scanning techniques, *Rendiconti Lincei*, 2011, **22**, 93–107.
6 F. Haselhuhn, S. Doyle and M. Kind, Synchrotron radiation X-ray diffraction study of the particle formation of pseudo-polymorphic calcium oxalate, *J. Cryst. Growth*, 2006, **289**, 727–733.
7 M. Kucher, T. Beierlein and M. Kind, *In situ* WAXS synchrotron radiation study on particle formation of precipitated barium sulfate, *AIChE J.*, 2008, **54**, 1178–1188.
8 B. Marmiroli, G. Grenci, F. Cacho-Nerin, B. Sartori, P. Laggner, L. Businaro and H. Amenitsch, Experimental set-up for time resolved small angle X-ray scattering studies of nanoparticles formation using a free-jet micromixer, *Nucl. Instrum. Methods Phys. Res., Sect. B*, 2010, **268**, 329–333.
9 W. Schmidt, P. Bussian, M. Lindén, H. Amenitsch, P. Agren, M. Tiemann and F. Schüth, Accessing Ultrashort Reaction Times in Particle Formation with SAXS Experiments: ZnS Precipitation on the Microsecond Time Scale, *J. Am. Chem. Soc.*, 2010, **132**, 6822–6826.
10 B. Clair, A. Ikni, W. Li, P. Scouflaire, V. Quemener and A. Spasojević-de Biré, A new experimental setup for high-throughput controlled non-photochemical laser-induced nucleation: application to glycine crystallization, *J. Appl. Crystallogr.*, 2014, **47**, 1252–1260.
11 A. Ikni, B. Clair, P. Scouflaire, S. Veesler, J.-M. Gillet, N. El Hassan, F. Dumas and A. Spasojević-de Biré, Experimental Demonstration of the Carbamazepine Crystallization from Non-photochemical Laser-Induced Nucleation in Acetonitrile and Methanol, *Cryst. Growth Des.*, 2014, **14**, 3286–3299.

12 W. Li, A. Ikni, P. Scouflaire, X. Shi, N. El Hassan, P. Gémeiner, J.-M. Gillet and A. Spasojević-de Biré, Non-Photochemical Laser-Induced Nucleation of Sulfathiazole in a Water/Ethanol Mixture, *Cryst. Growth Des.*, 2016, **16**, 2514–2526.
13 M. R. Ward, W. J. Jamieson, C. A. Leckey and A. J. Alexander, Laser-induced nucleation of carbon dioxide bubbles, *J. Chem. Phys.*, 2015, **142**, 144501.
14 M. R. Ward, A. M. Mackenzie and A. J. Alexander, Role of Impurity Nanoparticles in Laser-Induced Nucleation of Ammonium Chloride, *Cryst. Growth Des.*, 2016, **16**, 6790–6796.
15 M. R. Ward, S. McHugh and A. J. Alexander, Non-photochemical laser-induced nucleation of supercooled glacial acetic acid, *Phys. Chem. Chem. Phys.*, 2012, **14**, 90–93.
16 T. Hua, O. Gowayed, D. Grey-Stewart, B. A. Garetz and R. L. Hartman, Microfluidic Laser-Induced Nucleation of Supersaturated Aqueous KCl Solutions, *Cryst. Growth Des.*, 2019, **19**, 3491–3497.
17 Y. Liu, M. R. Ward and A. J. Alexander, Polarization independence of laser-induced nucleation in supersaturated aqueous urea solutions, *Phys. Chem. Chem. Phys.*, 2017, **19**, 3464–3467.
18 N. Javid, T. Kendall, I. S. Burns and J. Sefcik, Filtration Suppresses Laser-Induced Nucleation of Glycine in Aqueous Solutions, *Cryst. Growth Des.*, 2016, **16**, 4196–4202.
19 T. Tasnim, A. Goh, O. Gowayed, C. T. Hu, T.-Y. Chen, J. E. Aber and B. A. Garetz, Dendritic Growth of Glycine from Nonphotochemical Laser-Induced Nucleation of Supersaturated Aqueous Solutions in Agarose Gels, *Cryst. Growth Des.*, 2018, **18**, 5927–5933.
20 T. Sugiyama and S.-F. Wang, Manipulation of nucleation and polymorphism by laser irradiation, *J. Photochem. Photobiol., C*, 2022, **52**, 100530.
21 J. A. Jacob, S. Sorgues, A. Dazzi, M. Mostafavi and J. Belloni, Homogeneous Nucleation-Growth Dynamics Induced by Single Laser Pulse in Supersaturated Solutions, *Cryst. Growth Des.*, 2012, **12**, 5980–5985.
22 H. Y. Yoshikawa, Y. Hosokawa and H. Masuhara, Explosive crystallization of urea triggered by focused femtosecond laser irradiation, *Jpn. J. Appl. Phys., Part 2*, 2006, **45**, L23–L26.
23 B. Lindinger, R. Mettin, R. Chow and W. Lauterborn, Ice Crystallization Induced by Optical Breakdown, *Phys. Rev. Lett.*, 2007, **99**, 045701.
24 K. Nakamura, Y. Hosokawa and H. Masuhara, Anthracene crystallization induced by single-shot femtosecond laser irradiation: Experimental evidence for the important role of bubbles, *Cryst. Growth Des.*, 2007, **7**, 885–889.
25 A. Soare, R. Dijkink, M. R. Pascual, C. Sun, P. W. Cains, D. Lohse, A. I. Stankiewicz and H. J. M. Kramer, Crystal Nucleation by Laser-Induced Cavitation, *Cryst. Growth Des.*, 2011, **11**, 2311–2316.
26 T. H. Liu, T. Uwada, T. Sugiyama, A. Usman, Y. Hosokawa, H. Masuhara, T. W. Chiang and C. J. Chen, Single femtosecond laser pulse-single crystal formation of glycine at the solution surface, *J. Cryst. Growth*, 2013, **366**, 101–106.
27 J. Yu, J. Yan and L. Jiang, Crystallization of Polymorphic Sulfathiazole Controlled by Femtosecond Laser-Induced Cavitation Bubbles, *Cryst. Growth Des.*, 2021, **21**, 3202–3210.
28 N. Nagalingam, A. Raghunathan, V. Korede, C. Poelma, C. S. Smith, R. Hartkamp, J. T. Padding and H. B. Eral, Laser-Induced Cavitation for Controlling Crystallization from Solution, *Phys. Rev. Lett.*, 2023, **131**, 124001.
29 B. A. Garetz, J. E. Aber, N. L. Goddard, R. G. Young and A. S. Myerson, Nonphotochemical, Polarization-Dependent, Laser-Induced Nucleation in Supersaturated Aqueous Urea Solutions, *Phys. Rev. Lett.*, 1996, **77**, 3475–3476.
30 A. J. Alexander and P. J. Camp, Non-photochemical laser-induced nucleation, *J. Chem. Phys.*, 2019, **150**, 040901.
31 V. Korede, N. Nagalingam, F. M. Penha, N. van der Linden, J. T. Padding, R. Hartkamp and H. B. Eral, A Review of Laser-Induced Crystallization from Solution, *Cryst. Growth Des.*, 2023, **23**, 3873–3916.
32 Y. Liu, M. H. van den Berg and A. J. Alexander, Supersaturation dependence of glycine polymorphism using laser-induced nucleation, sonocrystallization and nucleation by mechanical shock, *Phys. Chem. Chem. Phys.*, 2017, **19**, 19386–19392.
33 H. Y. Yoshikawa, R. Murai, S. Sugiyama, G. Sazaki, T. Kitatani, Y. Takahashi, H. Adachi, H. Matsumura, S. Murakami, T. Inoue, K. Takano and Y. Mori, Femtosecond laser-induced nucleation of protein in agarose gel, *J. Cryst. Growth*, 2009, **311**, 956–959.
34 H. Y. Yoshikawa, R. Murai, H. Adachi, S. Sugiyama, M. Maruyama, Y. Takahashi, K. Takano, H. Matsumura, T. Inoue, S. Murakami, H. Masuhara and Y. Mori, Laser ablation for protein crystal nucleation and seeding, *Chem. Soc. Rev.*, 2014, **43**, 2147–2158.
35 J. O. Sindt, A. J. Alexander and P. J. Camp, Effects of nanoparticle heating on the structure of a concentrated aqueous salt solution, *J. Chem. Phys.*, 2017, **147**, 214506.
36 E. R. Barber, M. R. Ward and A. J. Alexander, The role of cavitation and gas bubbles in the non-photochemical laser-induced nucleation of sodium acetate, *CrystEngComm*, 2024, **26**, 3634–3642.
37 *CRC Handbook of Chemistry and Physics*, ed. D. Lide, CRC Press, Boca Raton, FL, 86th edn, 2005.
38 E. R. Barber, M. R. Ward, A. D. Ward and A. J. Alexander, Laser-induced nucleation promotes crystal growth of anhydrous sodium bromide, *CrystEngComm*, 2021, **23**, 8451–8461.
39 J. M. García-Ruiz and F. Otálora, in *Handbook of Crystal Growth*, ed. P. Rudolph, Elsevier, Boston, 2nd edn, 2015, pp. 1–43.
40 J. Schindelin, I. Arganda-Carreras, E. Frise, V. Kaynig, M. Longair, T. Pietzsch, S. Preibisch, C. Rueden, S. Saalfeld, B. Schmid, J.-Y. Tinevez, D. J. White, V. Hartenstein, K. Eliceiri, P. Tomancak and A. Cardona, Fiji: an open-source platform for biological-image analysis, *Nat. Methods*, 2012, **9**, 676–682.
41 E. A. Neppiras, Acoustic cavitation, *Phys. Rep.*, 1980, **61**, 159–251.
42 I. Akhatov, O. Lindau, A. Topolnikov, R. Mettin, N. Vakhitova and W. Lauterborn, Collapse and rebound of a laser-induced cavitation bubble, *Phys. Fluids*, 2001, **13**, 2805–2819.

43 X. Chen, R.-Q. Xu, J.-P. Chen, Z.-H. Shen, L. Jian and X.-W. Ni, Shock-wave propagation and cavitation bubble oscillation by Nd:YAG laser ablation of a metal in water, *Appl. Opt.*, 2004, **43**, 3251–3257.
44 D. Glaser and C. Polese, Cavitation bubble oscillation period as a process diagnostic during the laser shock peening process, *Appl. Phys. A: Mater. Sci. Process.*, 2017, **123**, 603.
45 D. Jasikova, P. Schovanec, M. Kotek and V. Kopecky, Comparison of cavitation bubbles evolution in viscous media, *EPJ Web Conf.*, 2018, **180**, 02038.
46 H. Lee, A. B. Gojani, T. Han and J. J. Yoh, Dynamics of laser-induced bubble collapse visualized by time-resolved optical shadowgraph, *J. Visualization*, 2011, **14**, 331–337.
47 I. Akhatov, N. Vakhitova, A. Topolnikov, K. Zakirov, B. Wolfrum, T. Kurz, O. Lindau, R. Mettin and W. Lauterborn, Dynamics of laser-induced cavitation bubbles, *Exp. Therm. Fluid Sci.*, 2002, **26**, 731–737.
48 X. Zhong, J. Eshraghi, P. Vlachos, S. Dabiri and A. M. Ardekani, A model for a laser-induced cavitation bubble, *Int. J. Multiphase Flow*, 2020, **132**, 103433.
49 A. N. Sabzeghabae, L. F. Devia-Cruz, E. Gutierrez-Herrera, S. Camacho-Lopez and G. Aguilar, Bubble dynamics of laser-induced cavitation in plasmonic gold nanorod solutions and the relative effect of surface tension and viscosity, *Opt. Laser Technol.*, 2021, **134**, 106621.
50 X. M. Liu, J. He, J. Lu and X. W. Ni, Effect of surface tension on a liquid-jet produced by the collapse of a laser-induced bubble against a rigid boundary, *Opt. Laser Technol.*, 2009, **41**, 21–24.
51 B. C. Knott, M. F. Doherty and B. Peters, A simulation test of the optical Kerr mechanism for laser-induced nucleation, *J. Chem. Phys.*, 2011, **134**, 154501.
52 M. Briard, C. Brandel and V. Dupray, Strong Enhancement of Nucleation Efficiency of Aqueous Ethylenediamine Sulfate Solutions by Nonphotochemical Laser-Induced Nucleation: Investigations on the Role of Solid Impurities in the Mechanism, *Cryst. Growth Des.*, 2023, **23**, 7169–7178.
53 S. Li, X. Xie, Q. Qiu and Y. Liu, Laser-induced nucleation of urea through the control of Insoluble Impurity, *Sci. Rep.*, 2024, **14**, 25777.

